Entropy **2013**, *15*, 1540-1566; doi:10.3390/e15051540

OPEN ACCESS

entropy

ISSN 1099-4300

www.mdpi.com/journal/entropy

Article

A Direct Numerical Simulation-Based Analysis of Entropy Generation in Turbulent Premixed Flames

Richard Farran and Nilanjan Chakraborty *

School of Mechanical and Systems Engineering, Newcastle University, Claremont Road, NE1 7RU Newcastle-Upon-Tyne, UK; E-Mail: richard.farran@ncl.ac.uk

* Author to whom correspondence should be addressed; E-Mail: nilanjan.chakraborty@ncl.ac.uk; Tel.: +44-191-222-3570; Fax: +44-191-222-8600.

Received: 8 January 2013; in revised form: 12 April 2013 / Accepted: 23 April 2013 / Published: 29 April 2013

Abstract: A compressible single step chemistry Direct Numerical Simulation (DNS) database of freely propagating premixed flames has been used to analyze different entropy generation mechanisms. The entropy generation due to viscous dissipation within the flames remains negligible in comparison to the other mechanisms of entropy generation. It has been found that the entropy generation increases significantly due to turbulence and the relative magnitudes of the augmentation of entropy generation and burning rates under turbulent conditions ultimately determine the value of turbulent second law efficiency in comparison to the corresponding laminar values. It has been found that the entropy generation mechanisms due to chemical reaction, thermal conduction and mass diffusion in turbulent flames strengthen with decreasing global Lewis number in comparison to the corresponding values in laminar flames. The ratio of second law efficiency under turbulent conditions to its corresponding laminar value has been found to decrease with increasing global Lewis number. An increase in heat release parameter significantly augments the entropy generation due to thermal conduction, whereas other mechanisms of entropy generation are marginally affected. However, the effects of augmented entropy generation due to thermal conduction at high values of heat release parameter are eclipsed by the increased change in availability due to chemical reaction, which leads to an increase in the second law efficiency with increasing heat release parameter for identical flow conditions. The combustion regime does not have any major influence on the augmentation of entropy generation due to chemical reaction, thermal conduction and mass diffusion in turbulent flames in comparison to corresponding laminar flames, whereas the extent of augmentation of entropy generation due to viscous dissipation in turbulent conditions in comparison to

corresponding laminar flames, is more significant in the thin reaction zones regime than in the corrugated flamelets regime. However, the ratio of second law efficiency under turbulent conditions to its corresponding laminar value does not get significantly affected by the regime of combustion, as viscous dissipation plays a marginal role in the overall entropy generation in premixed flames.

Keywords: direct numerical simulations; entropy generation; viscous diffusion; chemical reaction; thermal conduction; mass diffusion

1. Introduction

Entropy generation mechanisms play key roles in determining the second-law irreversibility in energy-conversion processes in internal combustion (IC) engines and gas turbines. Fundamental understanding of entropy generation mechanisms is pivotal to the efficient design of new generation IC engines and gas turbines. For this purpose, it is important to understand local behaviour of the different entropy generation mechanisms. Bejan [1] analysed the entropy generation mechanisms due to viscous action and heat transfer in channel flows. Local entropy generations due to heat and mass transfers in addition to viscous effects have been analyzed by San *et al.* [2] and Poulikakos and Johnson [3]. Puri [4] analyzed entropy generation in the context of droplet combustion and identified the optimum transfer number for the purpose of minimization of entropy generation. Hiwase *et al.* [5] subsequently proposed a theoretical model for exergy analysis for droplet-laden flows where the exergy loss is expressed as a function of Damköhler number and initial droplet temperature. Exergy analysis in spray combustion was analyzed by Datta and Som [6] for different conditions in terms of pressure, temperature, swirl number, droplet diameter and spray cone angle. Arpaci and Selamet [7] analyzed entropy generation in laminar premixed flames on a flat flame burner using analytical means and expressed the entropy generation rate in terms of the quenching distance. Nishida *et al.* [8] analysed entropy generation mechanisms in laminar hydrogen-air and methane-air premixed flames based on detailed chemistry based simulations and demonstrated the effects of equivalence ratio on the entropy generation in premixed flames. Different mechanisms of entropy generation in multi-component reacting systems have been identified in a number of previous analyses [8–15] on premixed and non-premixed combustion. Interested readers are referred to [15] for an extensive review of entropy generation in reactive system. It has been found that viscous dissipation, thermal conduction, mass diffusion and irreversible chemical reaction give rise to generation of entropy in reacting flows.

To date, most analyses on local entropy generation mechanism have been carried out for laminar flows [7,8,10–14] and relatively limited effort was given to the entropy generation mechanism in turbulent flames [14–17]. OKong'o and Bellan [16] and Safari *et al.* [17] discussed the importance of the local entropy transport in the context of combustion modelling especially for Large Eddy Simulations (LES). The present analysis is carried out following the theoretical basis provided by Safari *et al.* [17], but the statistical behaviors of the entropy generation mechanisms in response to the variations of combustion regime, heat release parameter and global Lewis number in turbulent premixed flames were not addressed in [17]. However, these effects have been adequately addressed in

this paper based on the analysis of Direct Numerical Simulations (DNS) data of statistically planar turbulent premixed flames.

In last two decades DNS has become an important tool for the analysis of turbulent flows where all the relevant length and time scales associated with turbulent flow processes are simulated without any recourse to physical approximations. Analysis of local entropy generation in turbulent flames based on DNS data has rarely been done in the existing literature. This void has been addressed here by analyzing entropy generation mechanisms in turbulent premixed flames based on three-dimensional compressible DNS data. As the nature of the fuel and the equivalence ratio of the mixture have significant influences on the entropy generation in turbulent premixed flames [8], a systematic parametric analysis based on DNS simulations has been carried out in this paper for different values of heat release parameter τ and global Lewis number Le (as the equivalence ratio, nature of the fuel and the level of preheating can be characterized by τ and Le). The heat release parameter τ and global Lewis number Le are defined as follows:

$$\tau = (T_{ad} - T_0)/T_0, \; Le = \lambda/(\rho c_p D) \tag{1}$$

where T_{ad}, T_0, λ, ρ, c_p and D are the adiabatic flame temperature, unburned gas temperature, thermal conductivity, gas density, specific heat at constant pressure and the mass diffusivity respectively. Moreover, turbulent flow conditions may have an influence on the entropy generation in turbulent premixed flames. Thus a DNS database of freely propagating statistically planar turbulent premixed flames with a range of values of heat release parameters τ (ranging from 2.3 to 4.5) and global Lewis numbers Le (ranging from 0.34 to 1.2) spanning both the corrugated flamelets and the thin reaction zones regimes, has been considered to analyze the different entropy generation mechanisms in turbulent premixed combustion. In this respect, the main objectives of the present investigation are as follows:

(1). To analyze the relative contributions of viscous dissipation, heat conduction, mass diffusion and chemical reaction towards the overall entropy generation in turbulent premixed combustion.
(2). To identify the effects of combustion regime, heat release parameter and global Lewis number on the different entropy generation mechanisms in turbulent premixed flames.

The rest of the paper will be organized as follows: the details related to the mathematical background and numerical implementation will be presented in the next two sections. Following this, results will be presented and subsequently discussed. Main findings will be summarized and conclusions will be drawn in the final section of this paper.

2. Mathematical Background

The volumetric rate of destruction of exergy in turbulent premixed flames due to irreversibilities can be expressed as:

$$\dot{E}_D = T_0 S'''_{gen} \tag{2}$$

where T_0 is the unburned gas temperature (which is considered to be the dead state in this analysis) and S'''_{gen} is the volumetric rate of entropy generation which can be obtained from the transport equation of entropy. The transport equation of entropy takes the following form [7–17]:

$$T\rho\frac{Ds}{Dt}=\rho\frac{De}{Dt}+p\rho\frac{D\vartheta}{Dt}-\sum_{\alpha=1}^{N}\mu_\alpha\rho\frac{DY_\alpha}{Dt} \tag{3}$$

where T, e, p, ρ, ϑ, μ_α and Y_α are the temperature, internal energy, pressure, density, specific volume, specific chemical potential of species α (per unit mass and not in terms of unit mole) and the mass fraction of species α respectively. The specific chemical potential μ_α is given by:

$$\mu_\alpha=h_\alpha-Ts_\alpha^0 \tag{4}$$

where $h_\alpha=h_\alpha^0+\int_{T_{ref}}^{T}C_{p\alpha}dT'$ is the specific enthalpy of species α, T_{ref} is the reference temperature, $C_{p\alpha}$ is the specific heat at constant pressure for species α, s_α^0 is the partial specific entropy which is given by:

$$s_\alpha^0=\frac{1}{M_\alpha}\left(\frac{\partial S}{\partial n_\alpha}\right)_{T,p,n_\beta(\beta\neq\alpha)} \tag{5}$$

where n_α and M_α are the number of moles and molecular mass of species α respectively and $S=ms=m\sum_{\alpha=1}^{N}Y_\alpha s_\alpha^0$ denotes the extensive entropy. Here all the species are considered to be ideal gases and for ideal gases s_α^0 can be expressed as:

$$s_\alpha^0=s_\alpha-R_\alpha\ln X_\alpha \tag{6}$$

where X_α, s_α and $R_\alpha=R^0/M_\alpha$ are the mole fraction, specific entropy and gas constant of the pure species α with R^0 being the universal gas constant. Using Equations. (2)–(6) the entropy transport equation takes the following form:

$$\frac{\partial(\rho s)}{\partial t}+\frac{\partial(\rho u_j s)}{\partial x_j}=\frac{1}{T}\left[\tau_{ij}\frac{\partial u_i}{\partial x_j}-\frac{\partial q_i}{\partial x_i}+\sum_{\alpha=1}^{N}\mu_\alpha\frac{\partial J_i^\alpha}{\partial x_i}-\sum_{\alpha=1}^{N}\mu_\alpha\dot{w}_\alpha\right] \tag{7}$$

where $\dot{w}_\alpha$ is the reaction rate for species α, which is negative (positive) for a reactant (product). The components of viscous stress tensor τ_{ij} and the *i*-th components of heat flux vector q_i and mass flux vector J_i^α are expressed using the Newton's law of viscosity, Fourier's law of heat conduction and Fick's law of mass diffusion respectively, in the following manner:

$$\tau_{ij}=\mu\left(\frac{\partial u_i}{\partial x_j}+\frac{\partial u_j}{\partial x_i}\right)-\frac{2}{3}\mu\delta_{ij}\left(\frac{\partial u_k}{\partial x_k}\right);\ q_i=-\lambda\frac{\partial T}{\partial x_i}+\sum_{\alpha=1}^{N}h_\alpha J_i^\alpha\ ;\ J_i^\alpha=-\rho D_\alpha\frac{\partial Y_\alpha}{\partial x_i} \tag{8}$$

where μ is the viscosity, u_i is the *i*-th component of velocity, λ is the thermal conductivity, Y_α is the mass fraction of species α and D_α is the mass diffusivity of species α. It is worth noting that Soret and Dufor effects are ignored here following several previous analyses on entropy generation in turbulent reacting flows [4–8,10–15,17]. Moreover, there have been several previous DNS based computational analyses [18–34], which ignored Dufor and Sorret effects without much loss of generality. These effects are not expected to play important roles in most hydrocarbon-air and hydrogen-air flames [35] unless extremely lean hydrogen-air flames are considered. Moreover, it is

worth noting that this analysis follows the theoretical basis provided by Safari *et al.* [17], which also ignored Soret and Dufor effects. Equation (8) can be utilised to recast Equation (7) as:

$$\frac{\partial(\rho s)}{\partial t}+\frac{\partial(\rho u_j s)}{\partial x_j}=\frac{1}{T}\left[\tau_{ij}\frac{\partial u_i}{\partial x_j}-\frac{1}{T}(q_i-\sum_{\alpha=1}^{N}h_\alpha J_i^\alpha)\frac{\partial T}{\partial x_i}+\sum_{\alpha=1}^{N}J_i^\alpha\left(\frac{\partial \mu_\alpha}{\partial x_i}+s_\alpha^0\frac{\partial T}{\partial x_i}\right)-\sum_{\alpha=1}^{N}\mu_\alpha\dot{w}_\alpha\right] \\ -\frac{\partial}{\partial x_i}\left[\frac{1}{T}(q_i-\sum_{\alpha=1}^{N}h_\alpha J_i^\alpha)+\sum_{\alpha=1}^{N}s_\alpha^0 J_i^\alpha\right] \tag{9}$$

where $$\sum_{\alpha=1}^{N}J_i^\alpha\left(\frac{\partial \mu_\alpha}{\partial x_i}+s_\alpha^0\frac{\partial T}{\partial x_i}\right)=\sum_{\alpha=1}^{N}\frac{J_i^\alpha}{T}\left(c_{p\alpha}\frac{\partial T}{\partial x_i}-T\frac{\partial s_\alpha^0}{\partial x_i}\right) \tag{10}$$

For ideal gas the derivative of Equation (5) takes the following form:

$$\frac{\partial s_\alpha^0}{\partial x_i}=\frac{1}{T}c_{p\alpha}\frac{\partial T}{\partial x_i}-\frac{R_\alpha}{X_\alpha}\frac{\partial X_\alpha}{\partial x_i}-\underbrace{\frac{R_\alpha}{p}\frac{\partial p}{\partial x_i}}_{\approx 0} \tag{11}$$

where the last term on the right hand side is often neglected for low Mach number flows [7–17] and thus Equation (11) can be used in Equation (10) to yield:

$$\sum_{\alpha=1}^{N}J_i^\alpha\left(\frac{\partial \mu_\alpha}{\partial x_i}+s_\alpha^0\frac{\partial T}{\partial x_i}\right)=\sum_{\alpha=1}^{N}R_\alpha J_i^\alpha\left(\frac{1}{X_\alpha}\frac{\partial X_\alpha}{\partial x_i}\right) \tag{12}$$

Thus, the last term on right hand side of Equation (9) can be expressed as:

$$-\frac{\partial}{\partial x_i}\left[\frac{1}{T}(q_i-\sum_{\alpha=1}^{N}h_\alpha J_i^\alpha)+\sum_{\alpha=1}^{N}s_\alpha^0 J_i^\alpha\right]=\frac{\partial}{\partial x_i}\left[\frac{\lambda}{T}\frac{\partial T}{\partial x_i}+\sum_{\alpha=1}^{N}\rho s_\alpha^0 D_\alpha\frac{\partial Y_\alpha}{\partial x_i}\right] \tag{13}$$

Here specific heats and mass diffusivities of all the species are taken to be identical (*i.e.*, $c_{pi}=c_p$ and $D_i=D$), which leads to:

$$\frac{\partial}{\partial x_i}\left[\frac{\lambda}{T}\frac{\partial T}{\partial x_i}+\sum_{\alpha=1}^{N}\rho s_\alpha^0 D_\alpha\frac{\partial Y_\alpha}{\partial x_i}\right]=\frac{\partial}{\partial x_i}\left(\rho D\frac{\partial s}{\partial x_i}\right)+\frac{\partial}{\partial x_i}\left(\frac{\lambda}{T}\left(1-\frac{1}{Le}\right)\frac{\partial T}{\partial x_i}\right) \tag{14}$$

Using Equations (12) and (14) in Equation (9) yields:

$$\frac{\partial(\rho s)}{\partial t}+\frac{\partial(\rho u_j s)}{\partial x_j}=\frac{\partial}{\partial x_i}\left(\rho D\frac{\partial s}{\partial x_i}\right)+\frac{\partial}{\partial x_i}\left(\frac{\lambda}{T}\left(1-\frac{1}{Le}\right)\frac{\partial T}{\partial x_i}\right)+T_1+T_2+T_3+T_4 \tag{15i}$$

where:

$$T_1=\frac{1}{T}\left[\tau_{ij}\frac{\partial u_i}{\partial x_j}\right];T_2=-\frac{1}{T}\sum_{\alpha=1}^{N}\mu_\alpha\dot{w}_\alpha;T_3=\frac{\lambda}{T^2}\frac{\partial T}{\partial x_j}\frac{\partial T}{\partial x_j}\text{ and }T_4=\sum_{\alpha=1}^{N}\rho D\frac{R_\alpha}{X_\alpha}\frac{\partial X_\alpha}{\partial x_i}\frac{\partial Y_\alpha}{\partial x_i} \tag{15ii}$$

The terms T_1, T_2, T_3 and T_4 denote entropy generation due to viscous action, chemical reaction, thermal conduction, and mass diffusion respectively. The volumetric rate of entropy generation is given by:

$$S'''_{gen}=T_1+T_2+T_3+T_4 \tag{16}$$

The second term on right hand side of Equation (15i) is identically zero for unity Lewis number cases (*i.e.*, $Le=1.0$). For non-unity Lewis number cases (*i.e.*, $Le\neq 1.0$) $\nabla\bullet[(\lambda/T)(1-Le^{-1})\nabla T]$ is

responsible for redistributing entropy and the volume integral of this term vanishes according to divergence theorem (*i.e.*, $\int_V \nabla \bullet [(\lambda/T)(1-Le^{-1})\nabla T]d\vartheta = \oint_A [(\lambda/T)(1-Le^{-1})\nabla T \bullet \vec{n}]dA = 0$ where dA and $d\vartheta$ are elemental surface area and volume respectively and $\vec{n}$ is the outward normal on the elemental surface) because ∇T vanishes both on unburned and burned gas sides of the flame brush.

The extent of augmentation of entropy generation rate due to viscous dissipation in turbulent flames can be quantified by using a quantity Q_{T1} which is defined as:

$$Q_{T1} = \int_V (T_1)_{turb} d\vartheta / \int_V (T_1)_{lam} d\vartheta \tag{17}$$

The subscripts "turb" and "lam" are used to refer to the values in turbulent and laminar flames respectively. Similarly, the augmentation of entropy generation rate due to T_2, T_3 and T_4 in turbulent conditions in comparison to the corresponding laminar flames can be characterized by Q_{T2}, Q_{T3} and Q_{T4}, which are defined as:

$$Q_{T2} = \int_V (T_2)_{turb} d\vartheta / \int_V (T_2)_{lam} d\vartheta \tag{18}$$

$$Q_{T3} = \int_V (T_3)_{turb} d\vartheta / \int_V (T_3)_{lam} d\vartheta \tag{19}$$

$$Q_{T4} = \int_V (T_4)_{turb} d\vartheta / \int_V (T_4)_{lam} d\vartheta \tag{20}$$

Based on Equations (17)–(20) the overall augmentation of entropy generation in turbulent flames in comparison to the corresponding laminar flames can be characterized as:

$$Q_T = \int_V (T_1 + T_2 + T_3 + T_4)_{turb} d\vartheta / \int_V (T_1 + T_2 + T_3 + T_4)_{lam} d\vartheta \tag{21}$$

Ideally DNS of turbulent premixed combustion should account for both three-dimensionality of turbulence and detailed chemical mechanism. However, until recently most combustion DNS simulations were carried out either in two-dimensions with detailed chemistry or in three-dimensions with simplified chemistry due to limitations in computer storage capacity. The CPU time for compressible DNS of turbulent reacting flows scales as: $w \sim n_l^3 n_t \,\mathrm{Re}_t^3 / Ma \times \phi^3 / Ka^{3/2}$ where Re_t is the turbulent Reynolds number, Ka is the Karlovitz number, ϕ is the number of grid points within the thermal flame thickness $\delta_{th} = (T_{ad} - T_0)/Max\left|\nabla T\right|_L$, n_l is the number of large-scale eddies within the domain and n_t is the number of eddy turn-over times, where the subscript *L* refers to the unstrained planar laminar flame quantities. The value of ϕ remains of the order of 10 and 20 for simple chemistry and detailed chemistry based DNS simulations respectively. Moreover, one needs to have $n_l \geq 3$ to obtain enough number of statistically independent turbulent velocity signals and $n_t \geq 1$ in order to ensure that the simulation results are independent of initial conditions. This suggests that detailed chemistry simulations, for a given set of values of n_l, n_t, Ka and Re_t, are several orders of magnitude more expensive than simple chemistry simulations, especially for hydrocarbon-air flames (e.g., 68 steps and 18 species are typically involved in detailed chemistry based methane-air flame simulations). Although three-dimensional DNS with detailed chemistry is becoming possible using multi-processor simulations [36], they still remain prohibitively expensive [36,37] for an extensive parametric analysis,

as carried out in this paper. Thus the chemical mechanism is simplified here using a generic single-step Arrhenius type chemical reaction (*i.e.*, $\text{Reactants} \rightarrow \text{Products}$) and the three-dimensionality of turbulence is simulated without any physical approximation. Single step chemistry has been used successfully to obtain fundamental physical insight and to develop high-fidelity models in several analyses in the past [18–34] and the same methodology has been followed here. In the context of simplified chemistry the species field is characterized by a reaction progress variable c, which can be defined in terms of a suitable reactant mass fraction Y_R as follows:

$$c = \frac{(Y_{R0} - Y_R)}{(Y_{R0} - Y_{R\infty})} \tag{22}$$

where subscripts 0 and ∞ denote the values in pure reactants and fully burned products. In the context of single step chemistry the term T_2 takes the following form as $\dot{w}_P = -\dot{w}_R$:

$$T_2 = -\frac{1}{T}\sum_{\alpha=1}^{N}\mu_\alpha \dot{w}_\alpha = -\frac{(\mu_P - \mu_R)}{T}\left|\dot{w}_R\right| \tag{23}$$

where subscripts P and R refer to quantities for products and reactants respectively. The difference between chemical potentials between products and reactants (*i.e.*, $(\mu_P - \mu_R)$) can be expressed as:

$$\mu_P - \mu_R = (g_P - g_R) + RT\ln(X_P / X_R) \tag{24}$$

In the present analysis the generic chemical mechanism is taken to represent typical hydro-carbon/hydrogen-air combustion where the number of moles does not change significantly as a result of chemical reaction. For such chemical reactions $(g_P - g_R)$ remains almost same as $(h_P - h_R) = -\tau c_p T_0$ (*i.e.*, $(g_P - g_R) \approx (h_P - h_R) = -\tau c_p T_0$) under globally adiabatic conditions. Based on the above theoretical background, the extent of irreversibility in turbulent premixed combustion can be expressed in the form of second-law efficiency η_{II} which can be defined in the following manner:

$$\eta_{II} = 1 - \frac{\int_V T_0 S'''_{gen} d\vartheta}{\int_V \left|\dot{w}_R\right|(g_R - g_P) d\vartheta} \tag{25}$$

The effects of combustion regime, heat release parameter and global Lewis number on the statistical behaviors of $Q_{T1}, Q_{T2}, Q_{T3}, Q_{T4}, Q_T$ and η_{II} will be discussed in detail in Section 4.2 of this paper.

It is important to note that the statistics of flame propagation and scalar gradient in turbulent premixed flames based on simple chemistry DNS are found to be in good agreement with the corresponding two-dimensional detailed chemistry DNS results (*i.e.*,. flame propagation statistics for simple chemistry DNS in [21,33] are in agreement with detailed chemistry DNS results in [38,39]; statistical behaviors of scalar gradient obtained from simple chemistry DNS in [24,40,41] are in agreement with detailed chemistry based results in [42–44] and [41] respectively). A comparison between References. [23] and [42] (see Figure 3a in [23] and Figure 1a in [42]) indicates that the variation of $\left|\dot{w}_R\right|$ with c obtained from single-step Arrhenius type chemistry is qualitatively similar to detailed chemistry based results for methane-air and hydrogen-air flames. It is worth noting that the simulations considered here mimic generic hydrocarbon-air flames (*e.g.*, methane-air flames) for $Le \approx 1.0$ cases, whereas $Le = 0.34$ and 0.6 cases represent hydrogen-air/hydrogen-blended hydrocarbon-air combustion.

In actual combustion process a change in equivalence ratio/fuel-type alters the values of heat release parameter τ and global Lewis number Le. Moreover, the level of pre-heating also affects the value of heat release parameter τ. It is worth noting that the global Lewis number Le is modified here independently of the other parameters for the purpose of identifying the effects of differential diffusion of heat and mass in isolation. However, it is difficult to assign a single characteristic Lewis number in a reacting flow field due to the presence of several species with different Lewis numbers. Often the Lewis number of deficient species is considered to be the global Lewis number characterizing the combustion process [35,45]. There have seen several studies in the past where the effects of differential diffusion of heat and mass have been analyzed by modifying the global Lewis number in isolation [18–26,46–48].The same approach has been adopted in this analysis. Equation (15ii) indicates that the entropy generation in premixed flames is dependent on the statistics of reaction rate $\dot{w}_\alpha$ and scalar gradients ∇T, ∇Y_α and ∇X_α, and as the statistics of reaction rate and scalar gradients are adequately captured by single-step chemistry, it can be expected that fundamental features of entropy generation in turbulent premixed flames can also be addressed using simple chemistry. The effects of regime of combustion, τ and Le on local entropy generation due to T_1, T_2, T_3 and T_4 will be analyzed in detail in Section 4 of this paper.

3. Numerical Implementation

In the present study a DNS database of freely propagating statistically planar turbulent premixed flames under decaying turbulence has been considered. The initial values for the root-mean-square (rms) turbulent velocity fluctuation normalized by unstrained planar laminar burning velocity u'/S_L and the integral length scale to flame thickness ratio l/δ_{th} are presented in Table 1 along with the values of Damköhler number $Da = l S_L / u' \delta_{th}$ (i.e. the ratio of the integral time-scale $t_f = l/u'$ to the chemical time-scale $t_c = \delta_{th}/S_L$), Karlovitz number $Ka = (u'/S_L)^{3/2}(l/\delta_{th})^{-1/2}$, turbulent Reynolds number $\mathrm{Re}_t = \rho_0 u' l / \mu_0$, heat release parameter $\tau = (T_{ad} - T_0)/T_0$ and Lewis number Le. Standard values are taken for Prandtl number Pr, ratio of specific heats $\gamma = c_p / c_v$ and the Zel'dovich number $\beta = T_{ac}(T_{ad} - T_0)/T_{ad}^2$ (*i.e.*, $\mathrm{Pr} = 0.7$, $\gamma = 1.4$, $\beta = 6.0$). The thermo-chemical parameters for cases A–G are chosen in such a manner so that the thermal diffusivity of the unburned gas α_T, specific heat at constant pressure c_p, unstrained laminar burning velocity S_L and unburned gas density ρ_0 remain the same for all cases considered here. It can be seen from Table 1 that the turbulent Reynolds numbers are comparable for all the cases considered here. The simulation domain is taken to be a rectangular parallelepiped of size $105\alpha_T/S_L \times 132\alpha_T/S_L \times 132\alpha_T/S_L$ ($42.18\alpha_T/S_L \times 42.18\alpha_T/S_L \times 42.18\alpha_T/S_L$) for case A (cases B-G), which is discretized by a Cartesian grid of $261\times128\times128$ ($230\times230\times230$) with uniform grid spacing in each direction. Each 230 × 230 × 230 simulation required approximately 2300CPU-hours using AMD Opteron 2214 2.2Ghz CPU processors and approximately 50 Gb per case for storage. In all cases the x_1-direction is taken to align with the direction of mean flame propagation, whereas the other directions are considered to be periodic. The domain boundaries in the x_1-direction in case A are taken to be turbulent inlet and outlet respectively. The domain boundaries in the direction of mean flame propagation in other cases are taken to be partially non-reflecting. The partially non-reflecting boundaries are specified using the Navier Stokes Characteristic Boundary Condition (NSCBC) technique [49]. According to NSCBC technique, the inviscid part of the Navier Stokes

equations are specified using a characteristic analysis based on a locally one-dimensional system $\partial A_i / \partial t + \lambda_i \partial A_i / \partial x_1 = \partial A_i / \partial t + L_i = 0$ (for i = 1–5) where $A_1 = p - \rho u_1 a$, $A_2 = p / \rho^\gamma$, $A_3 = u_2$, $A_4 = u_3$ and $A_5 = p + \rho u_1 a$, and the wave velocities λ_i are given by $\lambda_1 = u_1 - a$, $\lambda_2 = \lambda_3 = \lambda_4 = u_1$ and $\lambda_5 = u_1 + a$ with a being the local acoustic speed. The wave amplitude variations L_i directed into the domain need to be specified at the partially non-reflecting boundaries and the wave amplitude variations for the outgoing waves are estimated from internal solutions. For the incoming waves the following expressions for L_i s : $L_1 = \sigma_1 (p - p^{req})$, $L_2 = \sigma_2 (T - T^{req})$, $L_3 = \sigma_3 (u_2 - u_2^{req})$, $L_4 = \sigma_4 (u_3 - u_3^{req})$ and $L_5 = \sigma_5 (u_1 - u_1^{req})$ were considered, where $p^{req}, T^{req}, u_1^{req}, u_2^{req}$ and u_3^{req} are the target values of p, T, u_1, u_2 and u_3 respectively and σ_i s are the relevant relaxation parameters [49]. The values of $\partial \tau_{1j} / \partial x_1$ (for j = 1, 2 and 3) , $\partial q_{T1} / \partial x_1$ and $\partial q_c / \partial x_1$ are considered to be zero at the partially non-reflecting boundaries [49], where $q_{T1} = -k(\partial T / \partial x_1)$ and $q_c = -\rho D(\partial c / \partial x_1)$ are the heat and mass fluxes respectively. Interested readers are referred to [49] for a more detailed discussion on boundary conditions.

In case A, the spatial differentiation in the x_1-direction is carried out using a 6th order central difference scheme for the internal grid points but the order of the differentiation gradually deceases to one-sided 4th order difference scheme as the non-periodic boundaries are approached, whereas the differentiation in the transverse directions are carried out using a spectral method. For the other cases, a 10th order central-difference scheme is used for spatial discretisation for internal points in all directions which gradually decreases to a one-sided 2nd order scheme near non-periodic boundaries. The time advancement for all viscous and diffusive terms in case A is carried out using an implicit solver, whereas the convection terms in case A and all the terms in all other cases are time advanced using a low-storage third order Runge-Kutta method [50]. For all cases, the flame is initialized by a steady unstrained planar laminar flame solution, and the turbulent velocity fluctuation field is specified using an initially homogeneous isotropic field generated using a pseudo-spectral method [51]. The grid spacing is determined by the resolution of the flame structure, and about 10 grid points are kept within the thermal flame thickness $\delta_{th} = (T_{ad} - T_0) / Max|\nabla T|_L$ for all cases considered here. Case A represents the corrugated flamelets regime combustion (*i.e.*, $Ka < 1$) [52], whereas other cases represent the thin reaction zones regime combustion (*i.e.*, $Ka > 1$) [52]. The values of heat release parameter τ are different for cases A, B and C-G. The Karlovitz number can be taken to scale as [52]:

$$Ka \sim \frac{\delta_{th}^2}{\eta^2} \tag{26}$$

where η is the Kolmogorov length scale. Equation (26) suggests that the energetic turbulent eddies cannot penetrate into the flame in the corrugated flamelets regime combustion, whereas turbulent eddies are likely to penetrate into the preheat zone in the thin reaction zones regime combustion. However, the Kolmogorov length scale η remains greater than the reaction zone thickness in the thin reaction zones regime combustion so that chemical reaction can be sustained.

In all cases flame-turbulence interaction takes place under decaying turbulence. Under decaying turbulence, simulations should be carried out for at least $t_{sim} = Max(t_f, t_c)$, where $t_f = l / u'$ is the initial eddy turn over time and $t_c = \delta_{th} / S_L$ is the chemical time scale. The simulation in case A was run for about four initial eddy turn over times ($t_{sim} \sim 4\tau_f = 4l / u'$), whereas simulations were run for a time $3.0 t_f$ in cases B–G. The aforementioned simulation times remain either greater than (cases A) or equal

to (cases B–G) one chemical time scale and are comparable to several previous analyses [18–35,38–44]. The turbulent kinetic energy and its dissipation rate in the unburned gas ahead of the flame were not varying significantly with time when statistics were extracted and the qualitative nature of the statistics was found to have remained unchanged since $t = 1.5l/u'$ for all cases. The values of u'/S_L in the unburned reactants ahead of the flame at the time when statistics were extracted decreased by about 52% and 50%, of the initial values in cases A and B-G respectively. The values of l/δ_{th} have increased from their initial values by a factor of about 1.10 and 1.7 for cases A and B-G respectively, but there are still enough number of turbulent eddies on each side of the computational domain.

In Section 4 the Reynolds averaged values of T_1, T_2, T_3 and T_4 will be presented. For statistically planar flames the Reynolds/Favre averaged quantities are considered to be functions of the distance along the direction of mean flame propagation (x_1 direction), and are evaluated by ensemble averaging the relevant quantities in transverse directions ($x_2 - x_3$ planes). The statistical convergence of the Reynolds/Favre averaged quantities are assessed by comparing the corresponding values obtained using half of the sample size in the transverse directions using a distinct half of the domain, with those obtained based on full sample size. Both qualitative and quantitative agreements between these sets of values are found to be satisfactory. In the next section, only the results obtained based on full sample size will be presented for the sake of brevity.

Table 1. List of initial turbulence and combustion parameters for the present DNS database.

Case	u'/S_L	l/δ_{th}	Re_t	Da	Ka
A	1.41	9.64	56.7	6.84	0.54
B-G	7.5	2.45	47.0	0.33	13.17
Le = 1.0 (A, B, F) 0.34 (C),0.6 (D), 0.8 (E) and 1.2 (G). τ = 2.3 (A), 3.0 (B), 4.5 (C–G)					

Figure 1. Distributions of $S'''_{gen} \times \alpha_T / (\rho_0 S_L^2 c_p)$ in the central $x_1 - x_2$ plane for cases (a–g) A–G at the time when the statistics were extracted. The white lines indicate reaction progress variable *c* contours from *c* = 0.1 to 0.9, from left to right, in steps of 0.2.

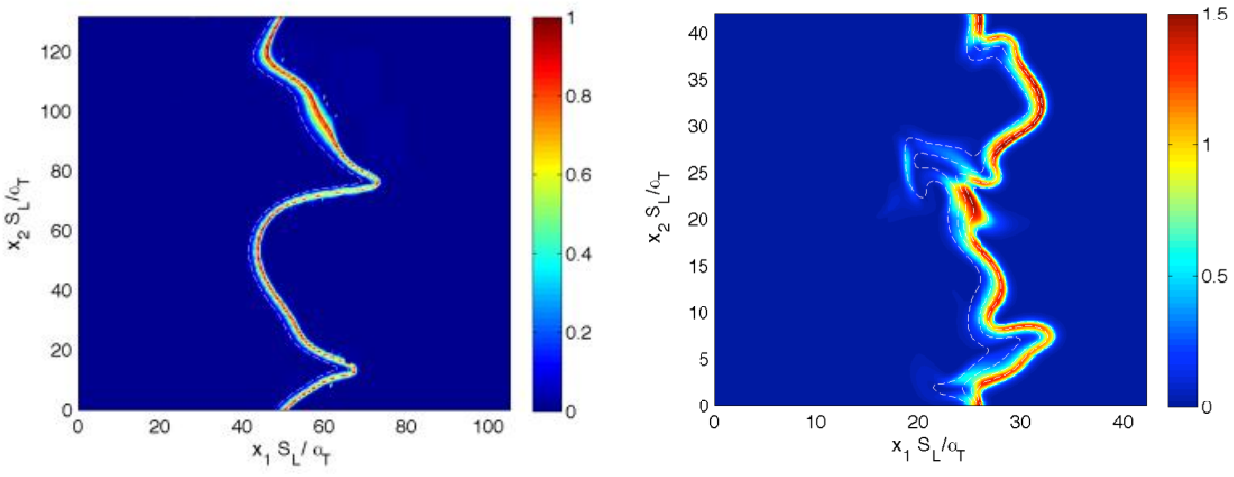

(a) **(b)**

Figure 1. *Cont.*

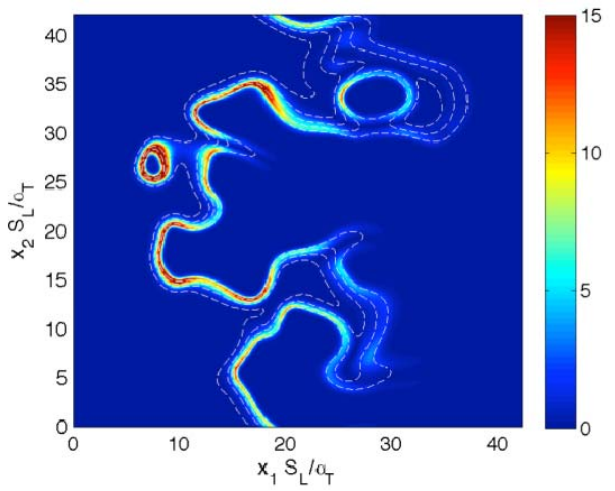

(c)

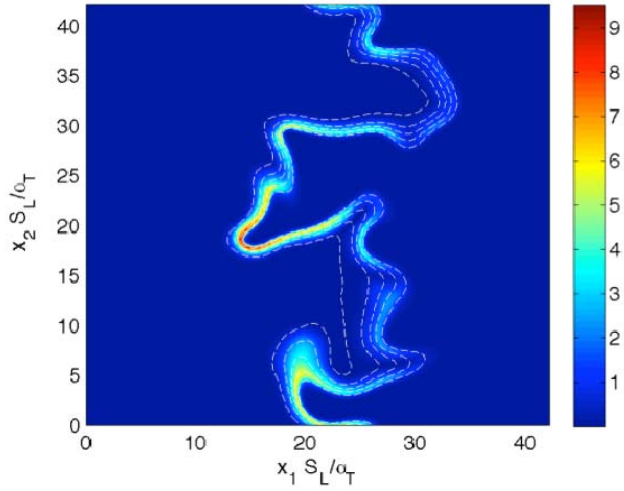

(d)

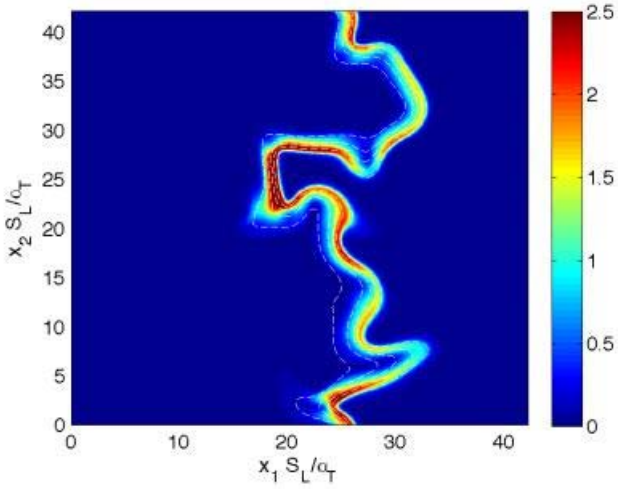

(e)

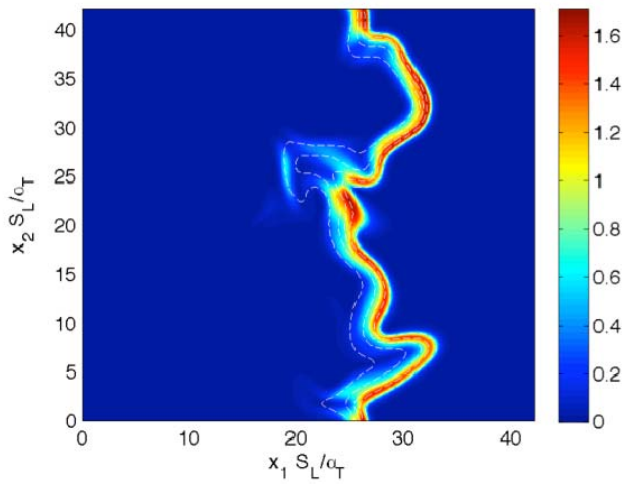

(f)

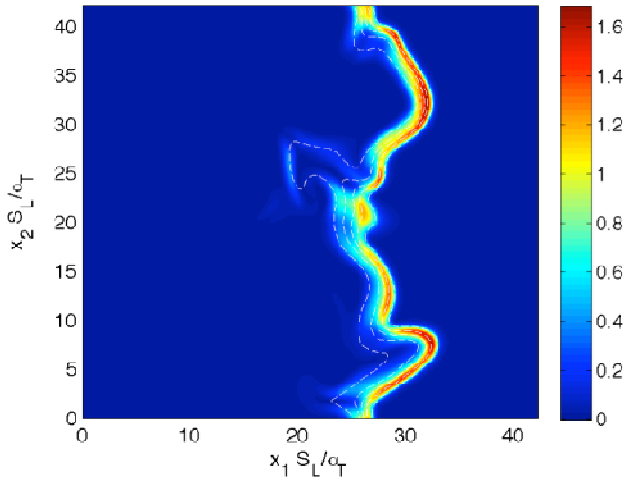

(g)

4. Results and Discussion

4.1. Relative Contributions of Entropy Generation Mechanisms in Turbulent Premixed Flames

The local distributions of $S'''_{gen} \times \alpha_T / \rho_0 S_L^2 c_p$ in the central $x_1 - x_2$ plane at the time when statistics were extracted are shown in Figure 1a–g for all cases considered here. The contours of c from 0.1 to 0.9 (in steps of 0.2 from left to right) are also shown in Figure 1a–g. It can be seen from Figure 1a that the contours of c are parallel to each other in case A because turbulent eddies do penetrate into the flame structure in the corrugated flamelets regime combustion [52]. By contrast, turbulent eddies penetrate into the preheat zone in the thin reaction zones regime flames (*i.e.*, cases B–G) and cause unsteady fluctuations, whereas the reaction zone (*i.e.*, $0.7 \le c \le 0.9$) remains relatively unperturbed. Figure 1c–g show that the extent of flame wrinkling increases with decreasing Le and this tendency is prevalent in the $Le << 1$ flames due to thermo-diffusive instabilities [18–26,46–48,53]. In the $Le << 1$ flames, fresh reactants diffuse faster into the reaction zone than the rate at which heat diffuses out, which gives rise to augmentation of burning rate and flame area generation in comparison to the corresponding unity Lewis number flame, due to the simultaneous presence of high reactant concentration and high temperature. Just the opposite mechanism is responsible for reduced burning rate and flame area generation in the $Le > 1.0$ flames in comparison to the corresponding unity Lewis number flame. The normalized turbulent flame speed S_T / S_L and normalized flame surface area A_T / A_L are presented in Table 2. The values of S_T / S_L have been evaluated by volume integrating the reaction rate $\dot{w} = -\dot{w}_R / (Y_{R0} - Y_{R\infty})$ using the expression $S_T = (1/\rho_0 A_P) \int \dot{w} d\vartheta$ where A_P is the projected area of the flame in the direction of mean flame propagation, while the values of A_T / A_L have been evaluated by volume integrating $|\nabla c|$ (*i.e.*, $\int |\nabla c| d\vartheta$) under both turbulent and laminar conditions. Table 2 shows that S_T / S_L and A_T / A_L increase strongly with decreasing Lewis number, and that this effect is particularly prevalent in the flames with $Le < 1$ due to the presence of thermo-diffusive instabilities [18–26,46–48,53].

Figure 1a–g show that the large values of $S'''_{gen} \times \alpha_T / \rho_0 S_L^2 c_p$ (where α_T is the thermal diffusivity in the unburned gas) are confined within the flame, and the entropy generation rate within the unburned reactants and fully burned products are much smaller than the values obtained within the flame (the value of entropy generation rate is not zero in unburned reactants and fully burned products).

Table 2. The values of normalized turbulent flame speed S_T / S_L and normalized flame surface area A_T / A_L when statistics were extracted.

Case	S_T / S_L	A_T / A_L
A	1.80	1.81
B	1.98	1.94
C	13.70	3.93
D	4.58	2.66
E	2.53	2.11
F	1.83	1.84
G	1.50	1.76

Figure 2. Variations of mean values of T_1, T_2, T_3 and T_4 conditional on bins of c (*i.e.*, $< T_1 >, < T_2 >, < T_3 >$ and $< T_4 >$) across the flame brush (a–g) A–G.

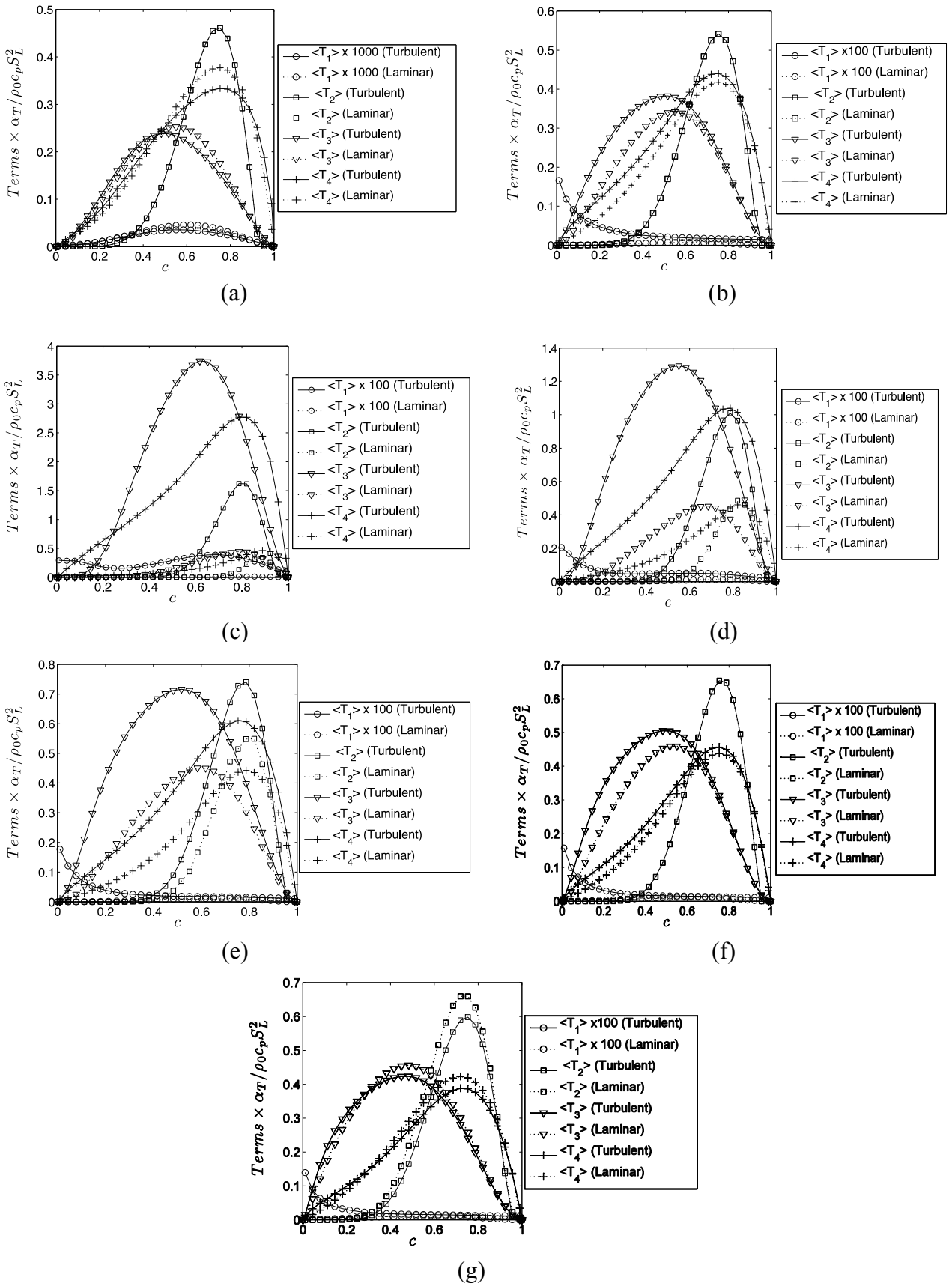

Figure 3. Variations of mean values of $\overline{T}_1, \overline{T}_2, \overline{T}_3$ and $\overline{T}_4$ with $\widetilde{c}$ across the flame brush: (a–g) A–G.

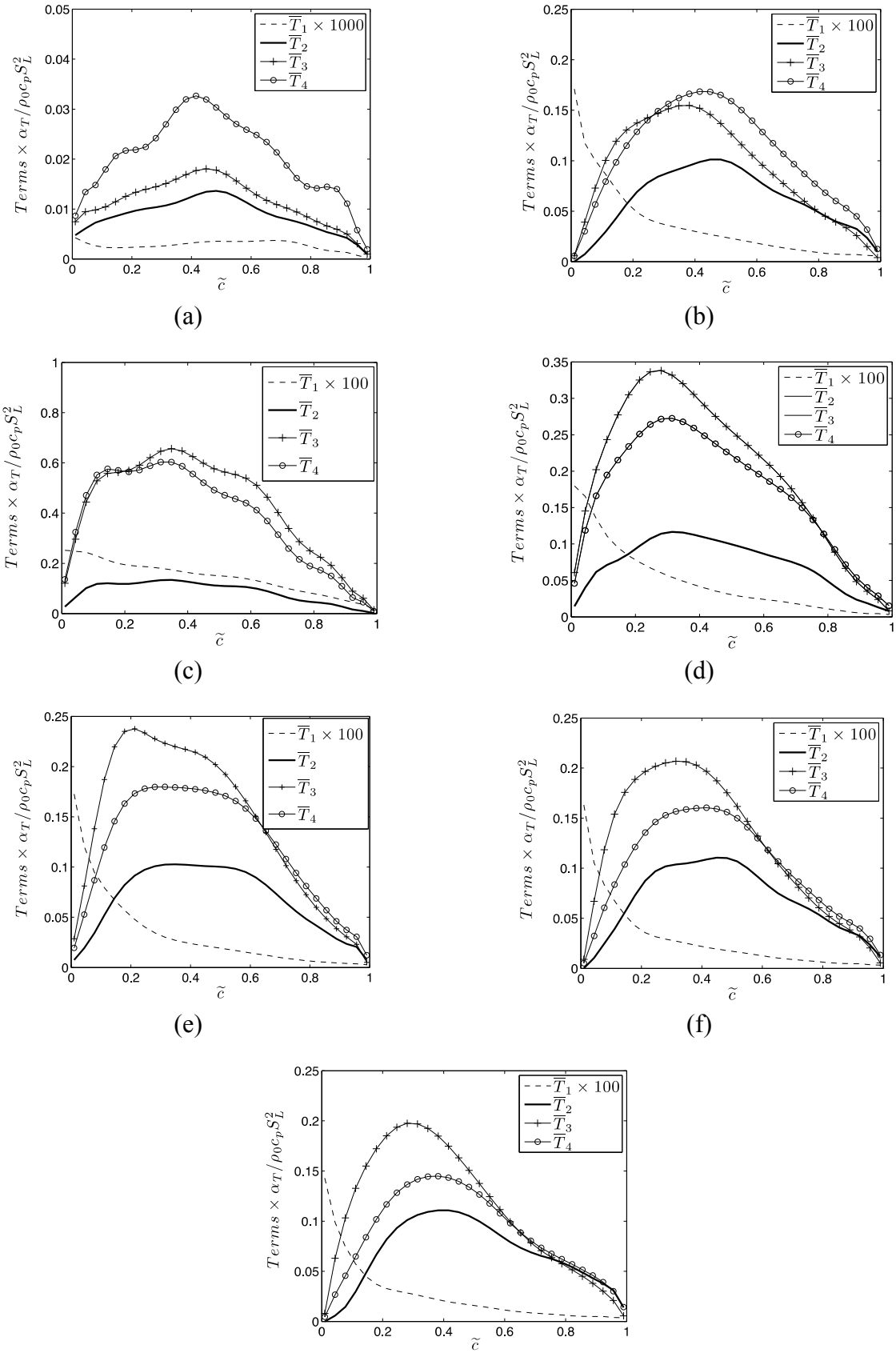

The values in unburned reactants and fully burned products are much smaller than the values obtained within the flame. Thus the colour bar in Figure 1a–g tends to show a value close to zero for entropy generation rate in unburned and fully burned gases.

It is worth noting that the terms T_2, T_3 and T_4 assume non-zero values within the flame, whereas T_1 remains active throughout the domain. In order to understand the relative contributions of different entropy generation mechanisms, the contributions of $< T_1 >, < T_2 >, < T_3 >$ and $< T_4 >$ (where $< Q >$ represents the ensemble averaged value of a quantity Q conditional on c values) across the flame brush are shown in Figure 2a–g for cases A–G respectively. The variations of the Reynolds averaged values of the different entropy generation mechanisms (*i.e.*, $\overline{T_1}, \overline{T_2}, \overline{T_3}$ and $\overline{T_4}$) with $\widetilde{c}$ for cases A-G are also presented in Figure 3a–g, respectively. It is evident from Figure 2a–g and Figure 3a–g that $< T_2 >, < T_3 >$ and $< T_4 >$ ($\overline{T_2}, \overline{T_3}$ and $\overline{T_4}$) remain major contributor to the entropy generation in all cases considered here. Moreover, the contribution of $< T_1 >$ ($\overline{T_1}$) remains several orders of magnitude smaller than the contributions of $< T_2 >, < T_3 >$ and $< T_4 >$ ($\overline{T_2}, \overline{T_3}$ and $\overline{T_4}$) for all cases considered here. This behaviour is found to be consistent with previous findings of Nishida *et al.* [8] in the context of detailed chemistry based laminar flame simulations. The contributions of $< T_1 >, < T_2 >, < T_3 >$ and $< T_4 >$ for the respective laminar flames are shown as functions of c in Figs. 2a-g, which also substantiate that the entropy generation due to viscous dissipation remains much smaller than the entropy generation due to chemical reaction, thermal conduction and species diffusion within the flame.

The observed behavior in Figure 3a–g (and also in Figure 2a–g) can be explained in terms of an order of magnitude analysis in the following manner:

$$\overline{T_1} \sim (\rho_0 c_p S_L^2 / \alpha_T) \times (\gamma - 1) Ma^2 \,;\, \overline{T_2} \sim (\rho_0 c_p S_L^2 / \alpha_T) \,;\, \overline{T_3} \sim (\rho_0 c_p S_L^2 / \alpha_T) \,;\, \overline{T_4} \sim (\rho_0 c_p S_L^2 / \alpha_T) \tag{27}$$

where $Ma = S_L / \sqrt{\gamma R T_0}$ is the flame Mach number and in Equation (27) the length scales associated with the thermal gradient $\partial T / \partial x_i$ and species gradients (*i.e.*, $\partial X_\alpha / \partial x_i$ and $\partial Y_\alpha / \partial x_i$) are taken to scale with the Zel'dovich flame thickness α_T / S_L, whereas both the viscous stress τ_{ij} and velocity gradient $\partial u_i / \partial x_j$ are taken to scale with S_L^2 / α_T following Swaminathan and Bray [30]. According to Tennekes and Lumley [54] the fluctuating parts of τ_{ij} and $\partial u_i / \partial x_j$ are taken to scale with $\rho_0 S_L \delta_{th} u' / \Lambda$ and u' / Λ (*i.e.*, $\mu(\partial u_i'' / \partial x_j) \sim \rho_0 S_L \delta_{th} u' / \Lambda$ and $\partial u_i'' / \partial x_j \sim u' / \Lambda$ where $u_i'' = u_i - \widetilde{u}_i$ and $\widetilde{u}_i = \overline{\rho u_i} / \overline{\rho}$ are Favre fluctuation and Favre mean values of i^{th} component of velocity) respectively where Λ is the Taylor micro-scale. The scaling arguments of Tennekes and Lumley [54] yield the following estimate of $\overline{T}_1$:

$$\overline{T_1} \sim (\rho_0 c_p S_L^2 / \alpha_T) \times (\gamma - 1) Ma^2 Ka^2 \sim (\rho_0 c_p S_L^2 / \alpha_T) \times (\gamma - 1) Ma^2 (\widetilde{\varepsilon} \delta_{th} / S_L^3) \tag{28}$$

where $\widetilde{\varepsilon} = \overline{\mu \partial u_i'' / \partial x_j \partial u_i'' / \partial x_j} / \overline{\rho}$ is the dissipation rate of turbulent kinetic energy $\widetilde{k} = \overline{\rho u_i'' u_i''} / 2\overline{\rho}$. It is clearly evident from Equation (28) that this scaling is only valid for turbulent flames, whereas $\overline{T_1}$ scaling according to Equation (27) is also valid for laminar flames as well. However, Equation (28) suggests that the contribution of T_1 is likely to be stronger in the thin reaction zones regime (*i.e.*, $Ka > 1$) than in the corrugated flamelets regime (*i.e.*, $Ka < 1$), which can be substantiated from Figures. 2 and 3. Moreover, Equations (27) and (28) indicate that the entropy generation due to viscous dissipation T_1 is expected to be much smaller than the entropy generation due to chemical reaction rate, thermal conduction, and species diffusion (*i.e.*, T_2, T_3 and T_4) for low Mach number (*i.e.*, $Ma << 1$) flames.

The scaling given by Equation (28) indicates that in case A (where $Ka<1$) the contribution of $<T_1>$ under turbulent conditions is likely to of the same order of $<T_1>$ under laminar conditions ($\because (\widetilde{\varepsilon}\delta_{th}/S_L^3)\sim Ka^2\sim O(1)$), whereas $<T_1>$ for turbulent flames is expected to be much greater than $<T_1>$ in the corresponding laminar flames in cases B-G (where $Ka>1$).

It is worth noting that the statistical behaviour of T_2 is directly proportional to $|\dot{w}_R|/T\propto \exp(-T_{ac}/T)/T$ (see Equation (23)) but $\exp(-T_{ac}/T)/T$ remains an increasing function of T (*i.e.*, $d[\exp(-T_{ac}/T)]/dT=[\exp(-T_{ac}/T)/T^2][\beta(1+\tau)^2/(\tau+\tau^2\Theta)-1]>0$ where $\Theta=(T-T_0)/(T_{ad}-T_0)$) suggesting the exponential temperature dependence of $\dot{w}_R$ dominates over the effects of $(1/T)$. Thus, it can be expected that the high values of T_2 are associated with high values of burning rate $|\dot{w}_R|$. Thus the values of $<T_2>$ and $\overline{T_2}$ are expected to increase with decreasing Le due to augmented burning rate for small values of global Lewis number (see Table 2).

It can further be seen from Figure 2a–g that the values of both $<T_3>$ and $<T_4>$ under turbulent conditions remain almost same as those in the laminar conditions in the unity Lewis number flames (e.g., cases A, B and F) but the values of $<T_3>$ and $<T_4>$ in turbulent flames are greater (smaller) than the corresponding laminar flame values for $Le<1.0$ ($Le>1.0$). In order to understand the above behaviour T_3 can alternatively be expressed as:

$$T_3=\frac{\rho_0 c_p\alpha_T\tau^2}{(1+\tau\Theta)^2}|\nabla\Theta|^2 \tag{29}$$

On the other hand, T_4 can be taken to scale as:

$$T_4\sim\rho_0 c_p\alpha_T(\gamma-1)|\nabla c|^2/\gamma Le \tag{30}$$

Equations (29) and (30) suggest that the statistics of $|\nabla\Theta|$ and $|\nabla c|$ are expected to play pivotal roles in the entropy generation due to T_3 and T_4 respectively. It is evident from the above discussion that

the statistical behaviors of dissipation rate of turbulent kinetic energy $\widetilde{\varepsilon}$, reaction rate $\dot{w}=|\dot{w}_R|/(Y_{R0}-Y_{R\infty})$ of reaction progress variable, $|\nabla\Theta|$ and $|\nabla c|$ in turbulent flames determine the extent of entropy generation due to T_1,T_2,T_3 and T_4 respectively along with the augmentation of flame surface area under turbulent conditions. The statistical behaviors of $\widetilde{\varepsilon}$, $\dot{w}$, $|\nabla\Theta|$ and $|\nabla c|$ will be discussed next in order to explain the observed behaviors of $<T_1>,<T_2>,<T_3>$ and $<T_4>$ ($\overline{T_1},\overline{T_2},\overline{T_3}$ and $\overline{T_4}$) in Figure 2a–g (Figure 3a–g).

4.2. Statistical Behaviors of $\widetilde{\varepsilon}$, $\dot{w}$, $|\nabla\Theta|$ and $|\nabla c|$ and Their Effects on Entropy Generation

4.2.1. Distribution of $\widetilde{\varepsilon}$

The variations of $\widetilde{k}/\widetilde{k}_0$ and $\widetilde{\varepsilon}/\widetilde{\varepsilon}_0$ with $\widetilde{c}$ for all cases considered here are shown in Figure. 4a,b respectively where $\widetilde{k}_0$ and $\widetilde{\varepsilon}_0$ are the values of turbulent kinetic energy and its dissipation rate at $\widetilde{c}=0.001$. It is worth noting that $\widetilde{k}_0$ and $\widetilde{\varepsilon}_0$ in case A are 36 and 390 times smaller than the corresponding values in cases B-G. It is also evident from Figure 4b that $\widetilde{\varepsilon}$ increases significantly with decreasing Le, which indicates that the magnitudes of $<T_1>$ and $\overline{T_1}$ are expected to increase with decreasing Lewis number Le (see Figures 2 and 3).

Figure 4. The variations of (a) $\tilde{k}/\tilde{k}_0$ and (b) $\tilde{\varepsilon}/\tilde{\varepsilon}_0$ with $\widetilde{c}$ for all cases considered here. The quantities $\widetilde{k}_0$ and $\widetilde{\varepsilon}_0$ are the values of turbulent kinetic energy and its dissipation rate at $\tilde{c}=0.001$.

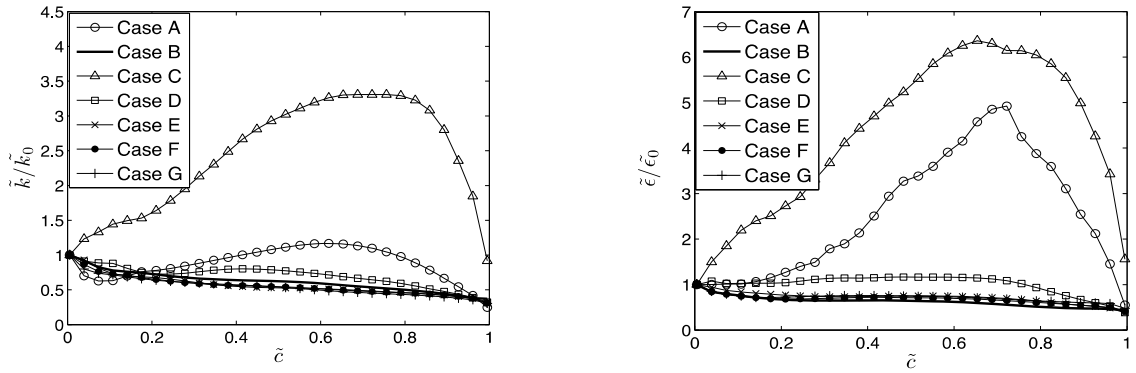

(a) (b)

A comparison between Figure 4a,b reveals that high values of $\widetilde{\varepsilon}$ in the $Le<<1.0$ flames are also associated with high $\widetilde{k}$ values. The augmentation of $\widetilde{k}$ in the $Le<<1.0$ flames arises due to strong flame-generated turbulence due to strong flame normal acceleration and interested readers are referred to Reference [26] for a detailed discussion. The effects of τ on $\widetilde{\varepsilon}$ are much weaker than the Lewis number effects (see Figure 4b) and thus τ has a marginal influence on the variation of $<T_1>$ and $\overline{T_1}$ within the flame brush (see Figure 2b,f and Figure3b,f).

4.2.2. Distribution of $\dot{w}$

The variations of $<\dot{w}>=<|\dot{w}_R|/(Y_{R0}-Y_{R\infty})>$ ($\overline{\dot{w}}=\overline{|\dot{w}_R|}/(Y_{R0}-Y_{R\infty})$) with c ($\widetilde{c}$) are shown in Figure 5a (Figure 5b), which indicates that the probability of finding high values of $|\dot{w}_R|$ increases significantly with decreasing Le. Thus, the magnitudes of $<T_2>$ and $<\dot{w}>=<|\dot{w}_R|/(Y_{R0}-Y_{R\infty})>$ in the flames with $Le=0.34$, 0.6 and 0.8 remain greater than the values of $<T_2>$ and $<\dot{w}>=<|\dot{w}_R|/(Y_{R0}-Y_{R\infty})>$ in the corresponding laminar flames (see Figure 2c□e). It is evident from Figure. 2a–g that the magnitude of $<T_2>$ in the $Le\geq 1.0$ (*i.e.*, $Le=1.0$ and 1.2) flames remains comparable to $<T_2>$ for laminar flames. However, flame surface area for turbulent flames is significantly greater than in the laminar flames, and, as a result, the volume integrated entropy generation due to T_2 in turbulent flames is expected to be greater than the values in the corresponding laminar flames.

4.2.3. Distributions of $|\nabla\Theta|$ and $|\nabla c|$

The variations of $<|\nabla\Theta|>$ and $<|\nabla c|>$ ($\overline{|\nabla\Theta|}$ and $\overline{|\nabla c|}$) with c ($\widetilde{c}$) are shown in Figure 6a,b (Figure 6c,d), which indicate that the probability of finding high values of $|\nabla\Theta|$ and $|\nabla c|$ increases significantly with decreasing Le. Moreover, the values of $<|\nabla\Theta|>$ and $<|\nabla c|>$ in turbulent flames are greater (smaller) than the corresponding laminar flame values for $Le<1.0$ ($Le>1.0$). The values of $<|\nabla\Theta|>$ and $<|\nabla c|>$ for both laminar and turbulent flames remain comparable in the case of $Le=1.0$. The physical explanations behind the augmentation (reduction) of $|\nabla\Theta|$ and $|\nabla c|$ in the $Le<1.0$ ($Le>1.0$) turbulent premixed flames in comparison to the corresponding laminar flames

have been discussed in detail elsewhere [24,25,42,43] and thus are not repeated here. Increasing probability of finding high values of $|\nabla\Theta|$ and $|\nabla c|$ with decreasing Le gives rise to increasing trends of $<T_3>$ and $<T_4>$ ($\overline{T_3}$ and $\overline{T_4}$) with decreasing Le for low Mach number non-unity Lewis number flames. According to Equation (29) an increase in τ gives rise to an increase in the magnitude of T_3 on a given c isosurface for the unity Lewis number flames and thus the magnitudes of $<T_3>$ and $\overline{T_3}$ in turbulent flames increase with increasing τ (see Figure 2b,f and Figure 3b,f). Similarly the magnitudes of T_3 in laminar flames increase with increasing τ (see Figure 2b,f).

Figure 5. (**a**) Variations of mean values of $\dot{w}\times\alpha_T/\rho_0 S_L^2 = |\dot{w}_R|/(Y_{R0}-Y_{R\infty})\times\alpha_T/\rho_0 S_L^2$ conditional on bins of c (*i.e.*, $<\dot{w}>\times\alpha_T/\rho_0 S_L^2 = <|\dot{w}_R|/(Y_{R0}-Y_{R\infty})>\times\alpha_T/\rho_0 S_L^2$) across the flame brush for all cases. (**b**) Variations of $\overline{\dot{w}}\times\alpha_T/\rho_0 S_L^2 = \overline{|\dot{w}_R|}/(Y_{R0}-Y_{R\infty})\times\alpha_T/\rho_0 S_L^2$ with $\widetilde{c}$ across the flame brush for all cases.

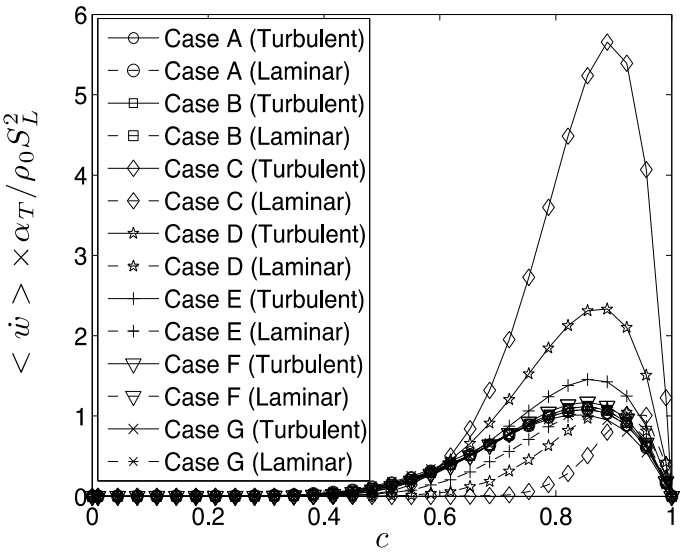

(a)

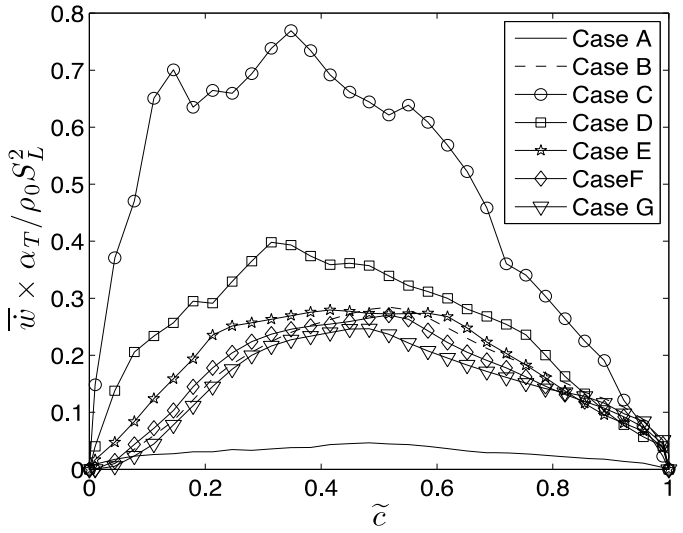

(b)

Figure 6. Variations of mean values of (a) $|\nabla\Theta|\times\alpha_T/S_L$ and (b) $|\nabla c|\times\alpha_T/S_L$ conditional on bins of c (*i.e.*, $<|\nabla\Theta|>\times\alpha_T/S_L$ and $<|\nabla c|>\times\alpha_T/S_L$) for all cases. Variations of (c) $\overline{|\nabla\Theta|}\times\alpha_T/S_L$ and (d) $\overline{|\nabla c|}\times\alpha_T/S_L$ with $\widetilde{c}$ across the flame brush.

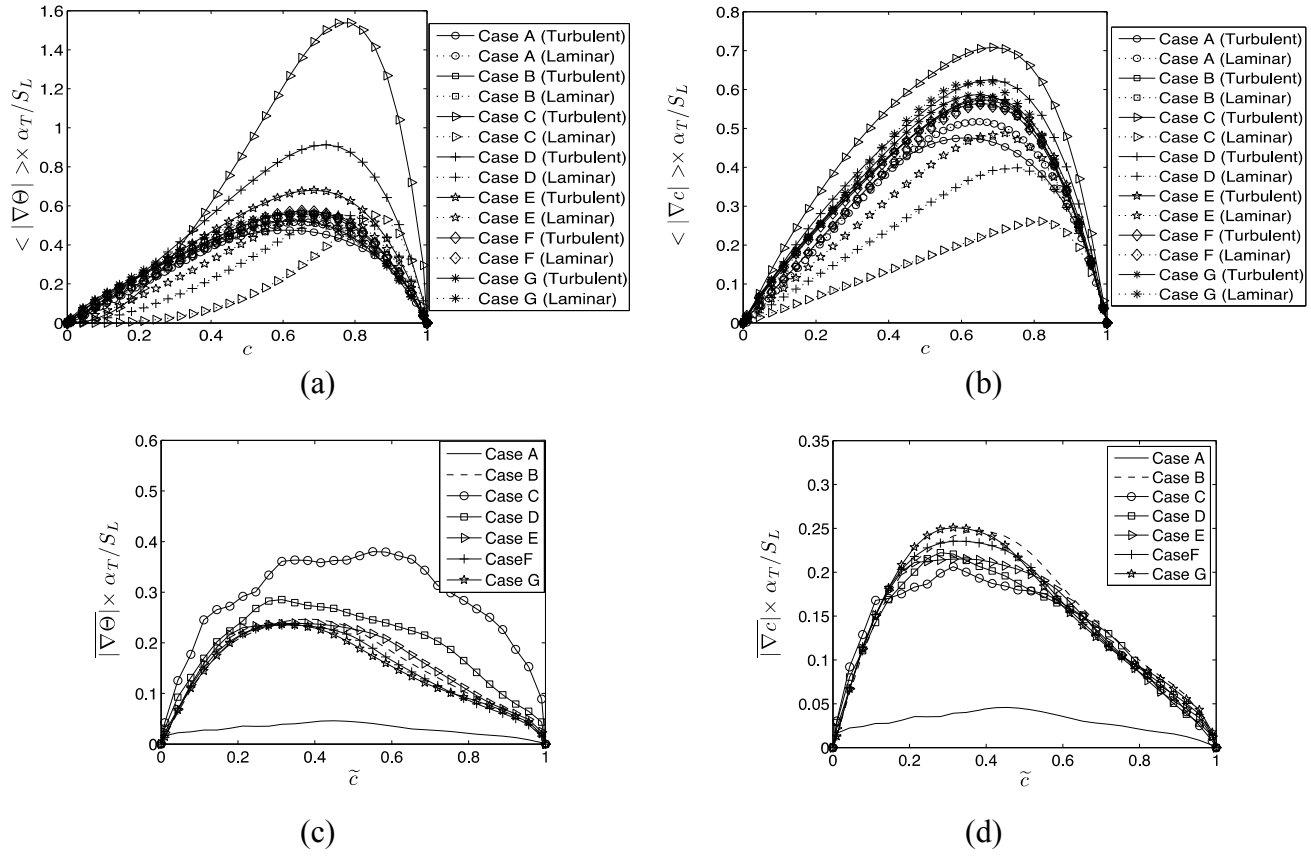

4.3. Entropy Generation Augmentation Rates $Q_{T1}, Q_{T2}, Q_{T3}, Q_{T4}$ and Q_T in Turbulent Flames

The statistical behaviors of $\widetilde{\varepsilon}$, $\dot{w}$, $|\nabla\Theta|$ and $|\nabla c|$, presented in Figures. 2–6, will be utilized here to analyze the augmentation of entropy generation rates $Q_{T1}, Q_{T2}, Q_{T3}, Q_{T4}$ and Q_T (see Equations. (19)–(21)) in turbulent flames, in comparison to the corresponding laminar flames. The values of $Q_{T1}, Q_{T2}, Q_{T3}, Q_{T4}$ and Q_T for cases A–G are presented in Figure. 7a–e respectively. It is evident from Figure 7a that Q_{T1} in the thin reaction zones regime flames assumes greater values than in the flame representing the corrugated flamelets regime, which is consistent with Equation (28), thus suggesting strengthening of the contribution of T_1 with increasing Ka. The flame surface area for turbulent premixed flames is greater than that in the corresponding laminar flames, which leads to a value of Q_{T1} much greater than unity (*i.e.*, $Q_{T1} >> 1$) even in case A where $< T_1 >$ values under both laminar and turbulent conditions remain of the same order (see Figure 2a). Augmentation of viscous dissipation rate $\widetilde{\varepsilon}$ with decreasing Le (see Figure 4b) gives rise to an increasing trend of Q_{T1} with decreasing Le. By contrast, a comparison between cases B and F shows an increase in Q_{T1} with decreasing τ. The values of $\widetilde{\varepsilon}$ (Ka) remain comparable (the same) for cases B and F and thus the higher value of Q_{T1} in case B than in case F originates principally due to greater extent of flame surface area generation by turbulence in case B than in case F (see Table 2).

Figure 7. Variations of (a) Q_{T1}, (b) Q_{T2} (c) Q_{T3}, (d) Q_{T4} and (e) Q_T for all cases considered here. (f) Percentage contributions to overall entropy generation by T_1, T_2, T_3 and T_4 for all cases.

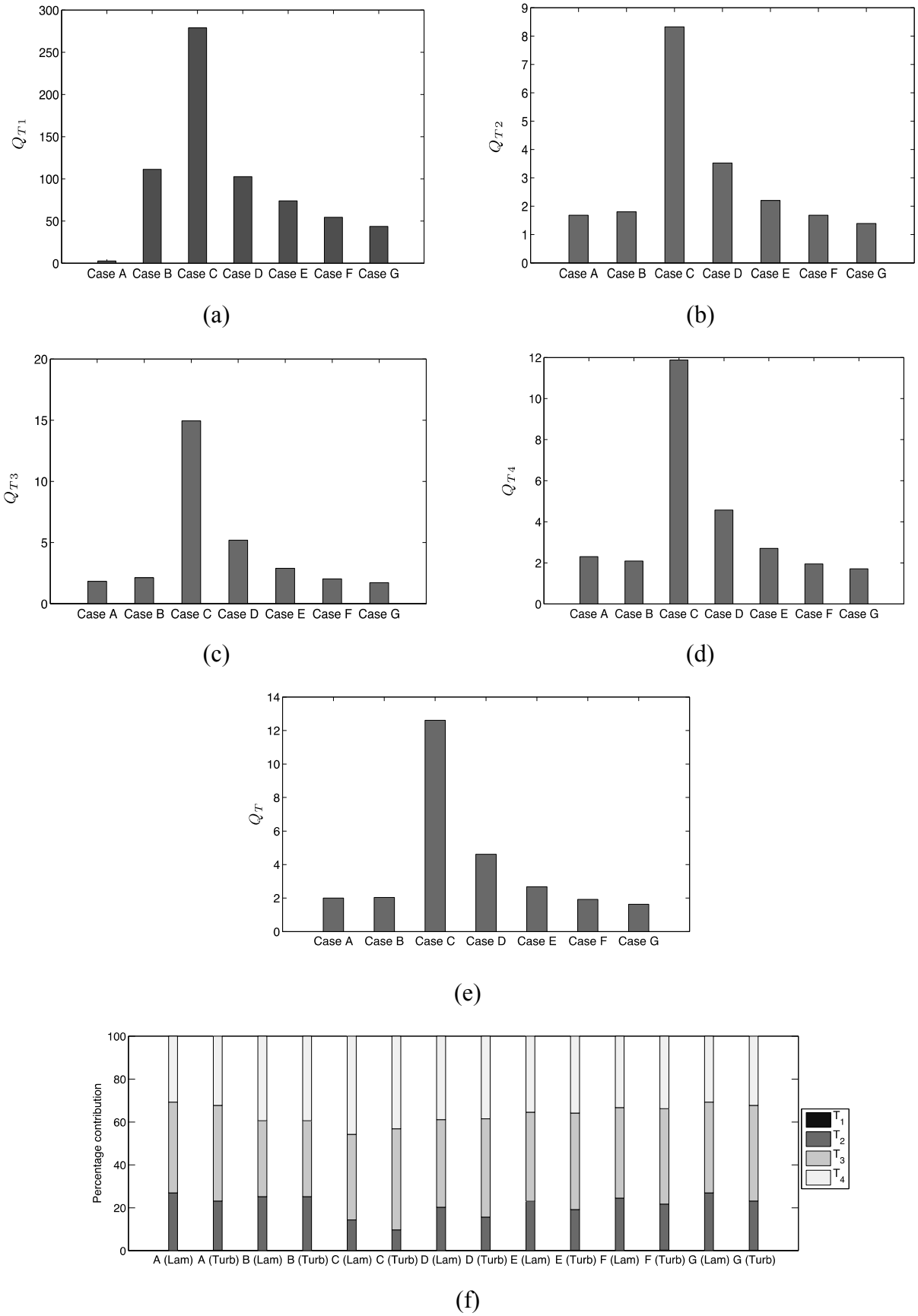

The variation of Q_{T2} in Figure 7b shows that Q_{T2} increases significantly with decreasing Le. A comparison between cases A, B and F in Figures 2,3 and 5 reveals that the effects of τ and the regime of combustion on the statistical behaviors on $< T_2 >$, $\overline{T}_2$, Q_{T2} and $\overline{\dot{w}}$ are much weaker than the effects of Le. This, in turn, leads to a significant increase in Q_{T2} with decreasing Le for turbulent premixed flames, as the magnitudes of $< \dot{w} >$ and $< T_2 >$ in turbulent flames in comparison to these values under laminar conditions increase with decreasing Le for the flames with $Le < 1$ (see Figure 5b and Figure 2c–e). In the $Le = 1.0$ and 1.2 flames, the magnitudes of $< \dot{w} >$ and $< T_2 >$ under turbulent conditions remain comparable to these values under laminar conditions (see Figure 5b and Figure 2f,g) so the augmentation of entropy generation due to chemical reaction (*i.e.*, $Q_{T2} > 1$) in these cases arise principally due to greater flame surface area of turbulent flames than in the corresponding laminar flames. As $\dot{w}$ remains uniform on a given c isosurface due to equivalence of c and T for low Mach number, globally adiabatic unity Lewis number flames, Q_{T2} values in cases A, B and F are determined by the augmentation of flame surface area. Comparable values of A_T / A_L between cases A, B and F (see Table 2) lead to comparable values of Q_{T2} in these cases. Thus, the regime of combustion does not significantly affect the statistical behavior of Q_{T2} in the cases considered here.

For low Mach number adiabatic unity Lewis number flames the definitions of c and non-dimensional temperature Θ become identical to each other so T remains uniform on a given c isosurface. Thus, the increase in flame surface area in turbulent flames leads to $Q_{T3} > 1.0$ and $Q_{T4} > 1.0$ in the unity Lewis number flames, as demonstrated in Figure 7c,d. Increasing probability of finding high values of $|\nabla\Theta|$ and $|\nabla c|$ with decreasing Le (see Figure 6a–d) gives rise to increasing trends of Q_{T3} and Q_{T4} (see Figure 7c,d) with decreasing Le for low Mach number non-unity Lewis number flames. Figure 7c,d demonstrate that the qualitative behaviors of Q_{T3} and Q_{T4} are not significantly affected by the regime of combustion, as the augmentation of flame surface area under turbulent conditions, in comparison to the corresponding laminar flames. remains comparable to each other for cases A, B and F (see A_T / A_L values in Table 2).

The foregoing discussion clearly indicates that all the different entropy generation mechanisms in premixed combustion are augmented under turbulent conditions, which can be confirmed from Figure 7e where the variations of Q_T are shown for all cases considered here. It is evident from Figure 7e that Q_T remains greater than unity (*i.e.*, $Q_T > 1.0$) for all cases considered here and Q_T increases significantly with decreasing Le. Moreover, Figure 7e shows that effects of τ and the regime of combustion on Q_T are much weaker than the effects of Le.

The percentage contributions to overall entropy generation by T_1, T_2, T_3 and T_4 for all cases are shown in Figure 7f for both turbulent and laminar conditions. It is evident that the contribution of T_1 remains small in comparison to the contributions of T_2, T_3 and T_4 under both laminar and turbulent conditions, which is consistent with previous findings of Nishida *et al.* [8] in the context of detailed chemistry based laminar flame simulations. It is evident from Figure 7f that the percentage contribution of T_2 to the overall entropy generation in turbulent flames decreases in comparison to the corresponding laminar flames. By contrast, the percentage contribution of T_3 to the overall entropy generation in turbulent flames increases in comparison to the corresponding laminar flames. The percentage contribution of T_2 (T_3) to the overall entropy generation decreases (increases) with decreasing Le. As the magnitude of T_3 increases with increasing τ (see Equation (29)) while the magnitudes of T_1, T_2 and T_4 are marginally affected by τ, the percentage contributions of T_2 and T_4 decrease with

increasing τ , whereas the percentage contribution of T_3 increases with increasing τ . As the qualitative behavior of the augmentation of entropy generation due to T_2, T_3 and T_4 under turbulent conditions are not significantly affected by the regime of combustion (see Figures. 4–6), and the contribution of T_1 remains negligible in comparison to the contributions of T_2, T_3 and T_4 under both laminar and turbulent conditions (see Figures 2,3), the percentage contribution of T_2, T_3 and T_4 to the overall entropy generation is not significantly affected by the regime of combustion (compare cases A, B and F in Figure 7f).

Figure 8. (**a**) Variations of η_{II} for all cases under both laminar and turbulent conditions. (**b**) Variations of the ratio of second law efficiencies under turbulent and laminar conditions (*i.e.*, $(\eta_{II})_{turb}/(\eta_{II})_{lam}$) for all cases.

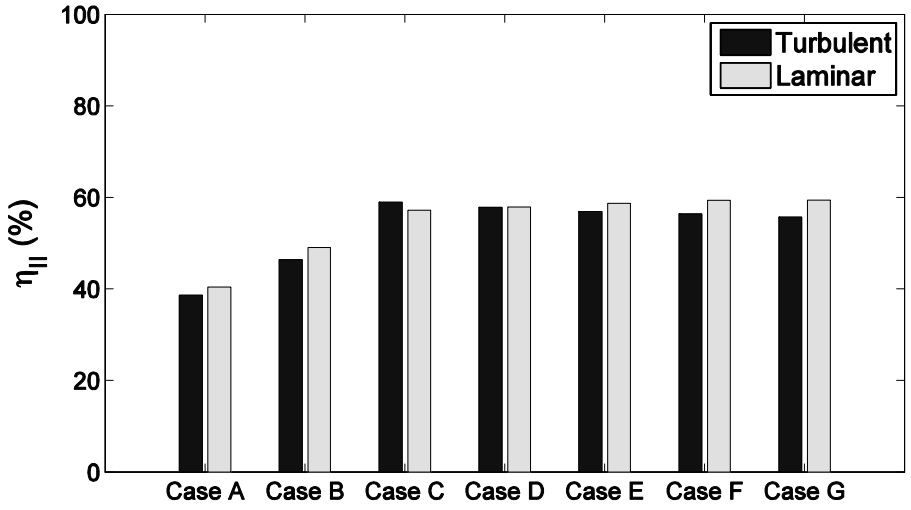

(a)

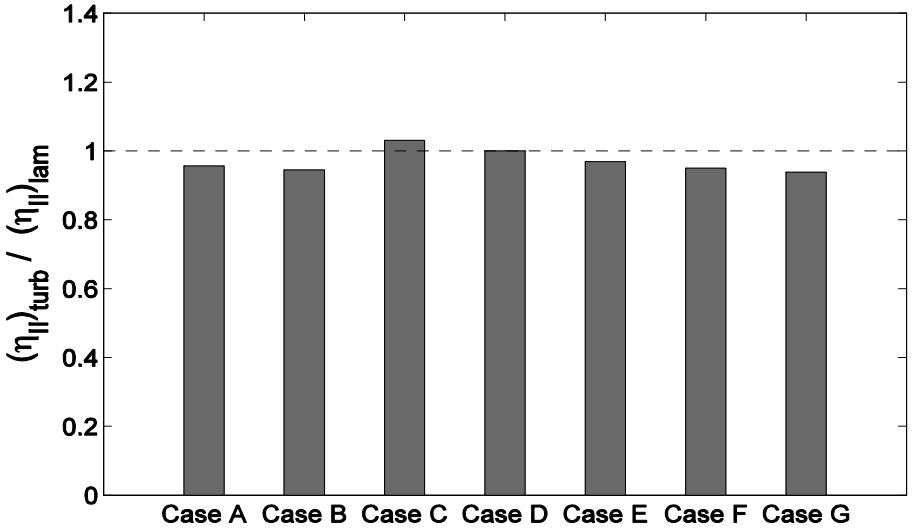

(b)

4.3. Statistical Behavior of Second-Law Efficiency η_{II}

The values of η_{II} for all cases under both laminar and turbulent conditions are shown in Figure 8a. The ratio of second law efficiencies under turbulent and laminar conditions (*i.e.*, $(\eta_{II})_{turb}/(\eta_{II})_{lam}$) for

all cases is shown in Figure 8b. It is evident from Figure 8a,b that η_{II} decreases under turbulent conditions for the flames with $Le \approx 1.0$ (*e.g.*, cases A, B, E–G). By contrast, the augmentation of burning rate in the $Le << 1$ cases (*e.g.* cases C and D) overcomes the enhancement of entropy generation under turbulent conditions, which gives rise to a greater value of η_{II} in turbulent flames, than in the corresponding laminar flames (see Figure 8a,b). Moreover, a comparison between cases B and F reveals that η_{II} increases with increasing τ. As $(g_R - g_P) \approx (h_R - h_P)$ in the present cases, η_{II} can alternatively be expressed as: $\eta_{II} \approx 1 - (1/\tau) \times \int_V S_{gen} d\vartheta / \int_V |\dot{w}_R| c_p d\vartheta$. Figures 2,3 and 5 demonstrate that the contribution of T_3 increases significantly with increasing τ, whereas τ has marginal influence on the statistical behaviors of $|\dot{w}_R|$, T_1, T_2 and T_4. By contrast, an increase in τ acts to increase η_{II} according to $\eta_{II} \approx 1 - (1/\tau) \times \int_V S_{gen} d\vartheta / \int_V |\dot{w}_R| c_p d\vartheta$, and this effect overcomes the effects of entropy generation augmentation due to T_3, giving rise to an increase in η_{II} with increasing τ (see Figure 8a). It can be seen by comparing the variations of Q_{T2}, Q_{T3} and Q_{T4} (see Figure 7) for cases A, B and F that the regime of combustion does not have any major influences on the augmentation of these modes of entropy generation under turbulent conditions in comparison to the corresponding laminar flames. However, Q_{T1} assumes much smaller value in the corrugated flamelets regime than in the thin reaction zones regime (see Figure 7a). However, the magnitude of T_1 contribution remains small in comparison to the magnitudes of T_2, T_3 and T_4 (see Figures 2,3), and thus the statistical behaviors of Q_T and $(\eta_{II})_{turb}/(\eta_{II})_{lam}$ do not get significantly affected by the regime of combustion, which can be seen from the comparison between cases A, B and F in Figures 7,8.

5. Conclusions

Different mechanisms of entropy generation in turbulent premixed flames have been analyzed in detail based on a simple chemistry DNS database with a range of different values of heat release parameter τ, global Lewis number Le spanning both the corrugated flamelets and thin reaction zones regimes of combustion. It has been found that the entropy generation increases under turbulent conditions. It has been found that the regime of combustion does not significantly affect the augmentation of entropy generation due to chemical reaction, thermal conduction and mass diffusion in turbulent flames in comparison to the corresponding laminar flames, whereas the entropy generation in turbulent flames due to viscous dissipation in comparison to the corresponding laminar flames is stronger in the thin reaction zones regime than in the corrugated flamelets regime. However, the regime of combustion does not significantly affect $(\eta_{II})_{turb}/(\eta_{II})_{lam}$, as viscous dissipation plays a marginal role in the overall entropy generation in premixed flames. The global Lewis number has been found have a profound influence on the entropy generation mechanism due to thermal conduction, chemical reaction and mass diffusion and the entropy generation by all the aforementioned mechanisms strengthen with decreasing Le. By contrast, τ significantly affects the entropy generation mechanism due to thermal conduction but other entropy generation mechanisms are marginally influenced. The entropy generation mechanism by the viscous dissipation remains negligible in comparison to the entropy generations due to chemical reaction, thermal conduction and mass diffusion for both laminar and turbulent conditions. Detailed physical explanations have been provided for the observed trends of entropy generation mechanisms in

response to the changes in τ and Le. The enhancement of entropy generation rate under turbulent conditions is superseded by the augmentation of burning rate for $Le<<1$ flames and thus the second law efficiency η_{II} for turbulent $Le=0.34$ and 0.6 flames are found to be either greater than (for $Le=0.34$) or comparable to ($Le=0.6$) the corresponding laminar flame values. By contrast, enhancement of entropy generation rate overcomes the augmented burning rate under turbulent conditions, which in turn leads to smaller value of η_{II} for turbulent flames, than in the corresponding laminar flames. Thus, a trade-off between heat release and second-law efficiency will be necessary for choosing an ideal fuel-air composition for a new industrial burner.

It is worth noting that this analysis has been carried out in the context of simplified chemistry and transport. The entropy generation in premixed flames is dependent on the statistical behaviors of reaction rate $\dot{w}_\alpha$ and scalar gradients ∇T, ∇Y_α and ∇X_α, and as the statistics of reaction rate and scalar gradients are adequately captured by single-step chemistry (see comparison between References. [23] and [42] for reaction rate statistics between simple and detailed chemistry; comparison between References. [21,33] and [38,39] for flame propagation statistics between simple and detailed chemistry; comparison between References. [24,40,41] and [41–44] for scalar gradient statistics between simple and detailed chemistry) it can be expected that the present findings based on simplified chemistry will be at least qualitatively valid in the context of detailed chemistry based analysis. However, the quantitative prediction of entropy generation for each individual case is likely to be different due to the effects of detailed chemistry and transport on μ_α. Thus, further analysis with detailed chemistry and transport will be necessary for more comprehensive DNS based analysis of entropy generation mechanisms in turbulent premixed combustion.

Acknowledgments

The financial assistance of EPSRC is gratefully acknowledged.

References

1. Bejan, A. A study of entropy generation in fundamental convective heat transfer. *ASME J. Heat Trans*. **1979**, *101*, 718–729.
2. San, J.Y.; Worek, W.M.; Lavan, Z. Entropy generation in combined heat and mass transfer, *Int. J. Heat Mass Trans.* **1987**, *30*, 1359–1369.
3. Poulikakos, D; Johnson, J.M. Second law analysis of combined heat and mass transfer phenomena in external flow. *Energy* **1989**, *14*, 67–73.
4. Puri, I.K. Second law analysis of convective droplet burning. *Int. J. Heat Mass Trans.* **1992**, *35*, 2571–2578.
5. Hiwase, S.D.; Datta, A.; Som, S.K. Entropy balance and exergy analysis of the process of droplet combustion. *J. Phys. D* **1998**, *31*, 1601–1610.
6. Som, S.K.; Datta, A., Thermodynamic irreversibilities and second law analysis in a spray combustion process. *Combust. Sci. Technol.* **1999**, *142*, 29–54.
7. Arpaci, V.S.; Selamet, A. Entropic efficiency of energy systems, *Combust. Flame.* **1988**,*73*, 251–259.
8. Nishida, K; Takagi, T.; Kinoshita, S., Analysis of entropy generation and exergy loss during combustion. *Proc. Combust. Inst.* **2002**, *29*, 869–874.

9. Hirschfelder, J.C.; Curtiss, C.F.; Bird, R.B. *Molecular Theory of Gases and Liquids*; Wiley: New York, NY, USA, 1954.
10. Datta, A., Entropy generation in a confined laminar diffusion flame. *Combust. Sci. Technol.* **2000**, *159*, 39–56.
11. Dunbar, W.R.; Lior, N., Sources of combustion irreversibility. *Combust. Sci. Technol.* **1994**, *103*, 41–61.
12. Teng, H.; Kinoshita, C.M.; Masutani, S.M.; Zhou, J. Entropy generation in multicomponent reacting flows. *J. Energ. Resour.—ASME* **1998**, *120*, 226–232.
13. Briones, A.M.; Mukhopadhay, A.; Aggarwal, S. Analysis of entropy generation in hydrogen-enriched methane—Air propagating triple flames. *Int. J. Hydrogen Energy* **2009**, *34*, 1074–1083.
14. Som, S.K.; Agrawal, G.K.; Chakraborty, S. Thermodynamics of flame impingement heat transfer. *J. Appl. Phys.* **2007**, *102*, 1–9.
15. Som, S.K.; Datta, A. Thermodynamic irreversibilities and exergy balance in combustion processes. *Prog. Energy Combust. Sci*. **2008**, *34*, 351–376.
16. O'Kongo, N.; Bellan, J., Entropy production of emerging turbulent scales in a temporal supercritical *n*-Heptane/Nitrogen three-dimensional mixing layer. *Proc. Combust. Inst.* **2002**, *28*, 497–502.
17. Safari, M; Sheikhi, M.R.; Janborogzi, M.; Metghalchi, M. Entropy transport equation in large eddy simulation for exergy analysis of turbulent combustion systems. *Entropy* **2010**, *12*, 434–444.
18. Ashurst, W.T.; Peters, N.; Smooke, M.D. Numerical Simulation of turbulent flame structure with non-unity Lewis number. *Combust. Sci. Technol.* **1987**, *53*, 339–375.
19. Haworth, D.C.; Poinsot, T.J. Numerical simulations of Lewis number effects in turbulent premixed flames. *J. Fluid. Mech*. **1992**, 244, 405–436.
20. Rutland, C.J.; Trouvé, A. Direct simulations of premixed turbulent flames with nonunity Lewis numbers. *Combust. Flame* **1993**, *94*, 41–57.
21. Chakraborty, N.; Cant, R.S. Influence of Lewis Number on curvature effects in turbulent premixed flame propagation in the thin reaction zones regime. *Phys. Fluids* **2005**, *17*,105105.
22. Chakraborty, N.; Cant, R.S. Influence of Lewis number on strain rate effects in turbulent premixed flame propagation in the thin reaction zones regime. *Int. J. Heat Mass Trans.* **2006**, *49*, 2158–2172.
23. Yuan, J.; Ju, Y.; Law, C.K. Coupled hydrodynamic and diffusional-thermal instabilities in flame propagation at small Lewis numbers, *Phys. Fluids* **2005**, *17*, 074106.
24. Chakraborty, N.; Klein, M. Influence of Lewis number on the surface density function transport in the thin reaction zones regime for turbulent premixed flames. *Phys. Fluids* **2008**, *20*, 065102.
25. Chakraborty, N.; Klein, M.; Swaminathan, N. Effects of Lewis number on reactive scalar gradient alignment with local strain rate in turbulent premixed flames. *Proc. Combust. Inst.* **2009**, *32*, 1409–1416.
26. Chakraborty, N.; Katragadda, M.; Cant, R.S. Effects of Lewis number on turbulent kinetic energy transport in turbulent premixed combustion. *Phys. Fluids* **2011**, *23*, 075109.
27. Veynante, D.; Trouvé, A.; Bray, K.N.C.; Mantel, T. Gradient and counter-gradient turbulent scalar transport in turbulent premixed flames. *J. Fluid Mech*. **1997**, *332*, 263–293.

28. Boger, M.; Veynante, D.; Boughanem, H.; Trouvé, A. Direct Numerical Simulation analysis of flame surface density concept for Large Eddy Simulation of turbulent premixed combustion. *Proc. Combust. Inst*. **1998**, *27*, 917–925.
29. Charlette, F.; Meneveau, C.; Veynante, D. A power-law flame wrinkling model for LES of premixed turbulent combustion. Part I: Nondynamic formulation and initial tests. *Combust. Flame* **2002**, *131*, 159–180.
30. Swaminathan, N.; Bray, K.N.C. Effect of dilatation on scalar dissipation in turbulent premixed flames. *Combust. Flame* **2005**, *143*, 549–565.
31. Swaminathan, N.; Grout, R. Interaction of turbulence and scalar fields in premixed flames, *Phys. Fluids.* **2006**, *18*, 045102.
32. Grout, R. An age extended progress variable for conditioned reaction rates. *Phys. Fluids* **2007**, *19*, 105107.
33. Han, I.; Huh, K.H. Roles of displacement speed on evolution of flame surface density for different turbulent intensities and Lewis numbers for turbulent premixed combustion. *Combust. Flame* **2008**, *152*, 194–205.
34. Han, I.; Huh, K.H. Effects of Karlovitz number on the evolution of the flame surface density in turbulent premixed flames. *Proc. Combust. Inst.* **2009**, *32*, 1419–1425.
35. Im, H.G.; Chen, J.H. Preferential diffusion effects on the burning rate of interacting turbulent premixed Hydrogen-Air flames. *Combust. Flame* **2002**, *131*, 246–258.
36. Babkovskaia, N.; Haugen, N.E.L.; Brandenburg; A. A high order public domain for direct numerical simulations of turbulent combustion. *J. Comp. Phys*. **2011**, *230*, 1–12.
37. Chen, J.H.; Choudhary, A.; de Supinski, B.; DeVries, M.; Hawkes, E.R.; Klasky, S.; Liao, W.K.; Ma, K.L.; Mellor-Crummey, J.; Podhorski, N.; *et al.* Terascale direct numerical simulations of turbulent combustion using S3D. *Comput. Sci. Discov.* **2009**, *2*, 015001.
38. Echekki, T.; Chen, J.H. Analysis of the Contribution of Curvature to Premixed Flame Propagation. *Combust. Flame* **1999**, *118*, 303–311.
39. Peters, N.; Terhoeven, P.; Chen, J.H.; and Echekki, T. Statistics of flame displacement speeds from computations of 2-D unsteady methane—Air flames. *Proc. Combust. Inst.* **1998**, *27*,833–839.
40. Chakraborty, N.; Hawkes, E.R. Determination of 3D flame surface density variables from 2D measurements: Validation using direct numerical simulation. *Phys. Fluids* **2011**, *23*, 065113.
41. Chakraborty, N.; Kolla, H.; Sankaran, R.; Hawkes, E.R.; Chen, J.H.; Swaminathan, N. Determination of three-dimensional quantities related to scalar dissipation rate and its transport from two-dimensional measurements: Direct numerical simulation based validation. *Proc. Combust. Inst.* **2013**, *34*, 1151–1162.
42. Chakraborty, N.; Hawkes, E.R.; Chen, J.H.; Cant, R.S. Effects of strain rate and curvature on Surface Density Function transport in turbulent premixed CH_4-air and H_2-air flames: A comparative study. *Combust. Flame* **2008,** *154*, 259–280.
43. Sankaran, R.; Hawkes, E.R.; Chen, J.H.; Lu, T.; Law, C.K. Structure of a spatially developing turbulent lean methane-air Bunsen flame. *Proc. Combust. Inst.* **2007**, *31*, 1291–1298.
44. Hawkes, E.R.; Sankaran, R.; Chen, J.H. Estimates of the three-dimensional flame surface density and every term in its transport equation from two-dimensional measurements. *Proc. Combust. Inst.* **2011**, *33*, 1447–1454.

45. Mizomoto, M.; Asaka, S.; Ikai, S.; Law, C.K. Effects of preferential diffusion on the burning intensity of curved flames. *Proc. Combust. Inst*. **1984**, *20*, 1933–1939.
46. Sivashinsky, G.I. Instabilities, pattern formation and turbulence in flames. *Annu. Rev. Fluid Mech.* **1983**, *15*, 179–199.
47. Clavin, P.; Williams, F.A. Effects of Lewis number on propagation of wrinkled flames in turbulent flow. *Prog. Aeronaut. Astronaut*. **1981**, *76*, 403–442.
48. Libby, P.A.; Linan, A.; Williams, F.A. Strained premixed laminar flames with non-unity Lewis numbers. *Combust. Sci. Technol.* **1983**, *34*, 257–293.
49. Poinsot, T.; Lele, S.K. Boundary conditions for direct simulation of compressible viscous flows. *J. Comp. Phys*. **1992**, *101*, 104–129.
50. Wray, A.A. *Minimal Storage Time Advancement Schemes for Spectral Methods*; Report No. MS 202 A-1; NASA Ames Research Center: California, CA, USA, 1990.
51. Rogallo, R.S. *Numerical Experiments in Homogeneous Turbulence*; NASA Technical Memorandum 91416; NASA Ames Research Center: California, CA, USA, 1981.
52. Peters, N. *Turbulent Combustion*; Cambridge University Press: Cambridge, UK, 2000.
53. Abdel-Gayed, R.G.; Bradley, D.; Hamid, M.; Lawes, M. Lewis number effects on turbulent burning velocity. *Proc. Combust. Inst*. **1984**, *20*, 505–512.
54. Tennekes, H.; Lumley, J.L. *A First Course in Turbulence*; MIT Press: Massachusetts, MA, USA, 1972.